IJST (2014) 38A2: 133-144
Iranian Journal of Science & Technology

http://ijsts.shirazu.ac.ir

Proposed optimization method for design of permanent magnet Guideways with high temperature superconductors

A. Hekmati

Electrical and Computer Engineering Department, Shahid Beheshti University,
Evin, Zip code: 1983963113, Tehran, Iran
E-mail: a_hekmati@sbu.ac.ir

Abstract

Superconducting materials are capable of trapping extremely high magnetic fields. This property and Meissner effect of superconductors causes a levitation force between bulk superconductors and a permanent magnet (PM). This levitation force has possible industrial applications such as Permanent Magnet Guideways (PMG). Because of the high price of permanent magnets, the optimization of PMG design is necessary and beneficial. A heuristic optimization method has been proposed for the optimum arrangement and dimensions of permanent magnets in different structures of PMGs, which guarantee the satisfactory levitation performance. Therefore, finite element simulation, based on the estimation of penetration depth and self-inductance of the superconductor disk, has been utilized. The variation of the PMG features, such as its dimensions and cost versus the system parameters, such as the levitation height and the superconductor disk characteristics have been presented as the optimization results. Based on the optimization process outputs, PMG prototypes have been fabricated and tested successfully.

Keywords*:* High temperature superconductor; levitation; optimization; permanent magnet guideway

1. Introduction

The purpose of the magnetic levitation is suspension with no mechanical supports. Using only ferromagnetic or paramagnetic materials it is impossible to provide a stable levitation against the gravity. Therefore, the possibility to achieve passive stable levitation between superconductors and permanent magnets can have many potentially applications (Brandt, 1988; Weinberger et al., 1991; Matsunaga et al., 2002; Minami et al., 1995; Kovalev et al., 2002; Oka et al., 2000; Yoo et al., 1998; Wang et al., 1999; Moon, 1994; Hull, 2000; Brandt, 1989; Ma et al., 2003). The high temperature superconductors (HTS) levitation has been widely used in the fields of the bearing (Nagaya et al., 2001; Oswald et al., 2002), energy storage (Deng, 2008) and the magnetic levitation transportation systems (Wang et al., 2002; Schultz et al., 2005; Wang et al., 2009; Zhang et al., 1998), and are particularly fit for the missile or launcher systems (Stumberger et al., 2004; Yang et al., 2006; Putman et al., 2005). The levitation and guidance is a result of the interaction between the permanent magnet guideway (PMG) and the onboard superconductor disk (SD), so PMG plays a key role in HTS Maglev systems and optimizing PMG is a direct and effective approach to improve the levitation performance of the vehicle. For any levitating system, and in particular the Maglev systems consisting of bulk superconductors and permanent-magnet guideways, the key aspect for a correct operation is the levitation force, which determines levitation height of the superconductor and is dependent on the parameters of both superconductor bulk and permanent-magnet guideway. The most important parameters of superconducting bulk are the dimensions, critical current density, cooling process of superconductor (Ren et al., 2003; Yang et al., 2007; Ma et al., 2008; Del-Valle et al., 2007; Kuehn et al., 2007; Cha et al., 1991; Wang et al., 2007; Del-Valle et al., 2008) and on the other hand, the number, size, lateral separation and magnetic parameters of the magnets are the most significant parameters of the permanent-magnet guideway (Del-Valle et al., 2007; Zheng et al., 2006; Cha et al., 1991; Wang et al., 2007; Andrade et al., 2003; Del-Valle et al., 2007). So far, much attention has been paid to the modeling of the levitated superconductor, which is advancing from 2D to 3D models (Rubinacci et al., 2004; Grilli et al., 2005). Numerical analysis on the influence of the applied field on the levitation and guidance force, and the guidance performance dependence on size parameters of superconductor and guideway (Song et al., 2007), are under extensive investigation. However, there is not a complete theoretical study that analyzes how the

Received: 7 May 2013 / Accepted: 16 April 2014

levitation force and height of the PMG systems depend upon the dimensions and geometry of the superconducting or guideway parts. In this work, the influence of the magnets arrangement on the levitation force of systems with translational symmetry formed by a superconductor and a guideway of permanent magnets is studied. Moreover, a method to assess the efficiency of PMGs and to determine the optimum PMG design is presented. With the results of this work, some guidelines are established on how the features of the superconductor and magnets of the system should be to achieve a large desired levitation force. For levitation force, many experimental investigations and numerical evaluations have been done (Alvaro et al., 2001; Tsuchimoto et al., 1994; Hashizume et al., 1996), and several groups have reported their theoretical and experimental results in recent years about the calculation and measurement of the hysteretic levitation force between a PM and an SD. In this paper the method presented by Komano et al., (2004) has been used for the levitation force calculation. The magnetic flux density of the PMG has been calculated via the 3D model of the PMG which has been implemented using FLUX3D.

In this paper, the exact magnetic field shape and the high precision calculation of the levitation force have been considered in the PMG optimization and an algorithm has been proposed for the optimum design determination of the PMG. The target is the most economical PM arrangement, which results in satisfactory levitation performance. The optimization algorithm considers the calculation of the levitation forces of the superconductor on different PMG structures and at different PMG cross sections. The optimization results contain the variation of the distinctive PMG features, such as its cost and width, versus the main parameters of the system such as the levitation height and the superconductor disk characteristics including its radius, height and critical current density. These results will provide basic analysis for the optimized HTS-PMG levitation systems.

2. PMG structures

In the present paper the HTS levitation system consists of a disk shaped HTS and the rectangular PMs. The HTS bulk disk in this study has the diameter of 8 mm and the height of 2 mm. The measurement of the critical current density, J_c, for the HTS bulk with the field trap method (Hekmati et al., 2012) shows the value of 10 A/mm^2.

Neodymium Magnets are made from an alloy containing the elements Neodymium, Iron and Boron (NdFeB) and are the strongest type of magnet commercially available and are manufactured in a wide range of shapes, sizes. It has reasonably been assumed in this study that the magnets have constant magnetization density. The cost of the magnets has been assumed proportional to the magnets volume which is a good assumption based on the market.

Three different guideway structures have been considered, as shown in Fig. 1. The magnetization directions of the magnets in these guideways have been illustrated in Fig. 2. At the structure I, a sole magnet forms a longitudinal sample of the PMG and the variable parameters are the width (w), the height (h) and the length (l), of each magnet and the distance of each magnet from the adjacent magnet (d), as shown in Fig. 1.a. At the structure II, the longitudinal sample of the PMG consists of three magnets: two side magnets with the width of w_s, length l_s and the height of h_s, and the longitudinal distance d_o between two adjacent side magnets, and a central magnet with the width of w_c, length of l_c and the height of h_c with the longitudinal and the latitudinal displacement of d_m and d_i, respectively, relative to the side magnets, as shown in Fig. 1.b. The longitudinal sample of the PMG at the structure III, is formed of four magnets: two central and two side magnets with the characteristic parameters as in structure II, except the latitudinal distance of d_c between the central magnets, as shown in Fig. 1.c. To investigate the optimum PMG dimensions, the levitation force has to be calculated for the three structures.

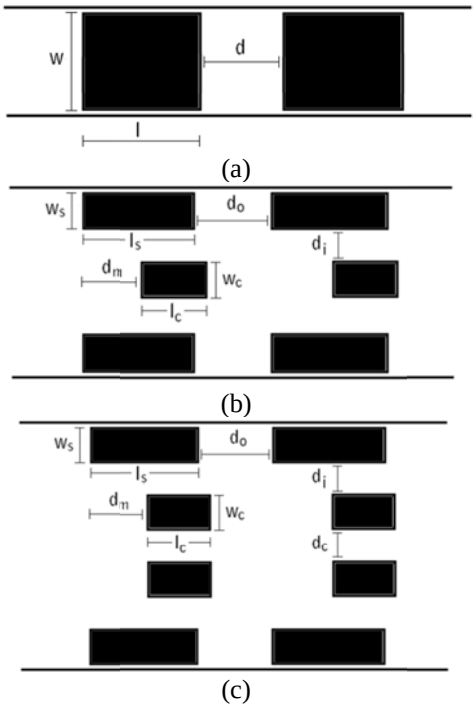

Fig. 1. The PMG structures considered, a) Structure I, b) Structure II, c) Structure III

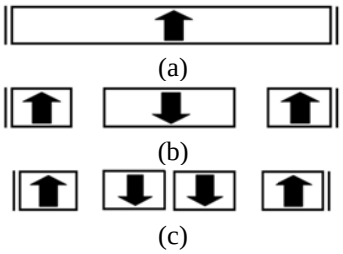

Fig. 2. The magnetization directions of the magnets in PMG, a) Structure I, b) Structure II, c) Structure III

3. Supercurrents distribution

In the process of imposing the external field to the superconductor bulk, the shielding current is induced to cancel the variation of the field in the bulk. To derive the conditions of lift, the supercurrent distribution in a field-cooled YBCO disk must be determined. We applied the Sand-pile model based on the Bean model in which the shielding current distribution is independent of the magnetic field. According to this model, the shielding current distribution, J_c, and the trapped magnetic field are related as (1), (Iwasa et al., 1997; Fukai et al., 2001; Tamegai et al., 1993; Nagashima et al., 1997; Fukai et al., 2000).

$$J_c = -\frac{1}{\mu_0}\frac{dB_{trapz}(r)}{dr} \tag{1}$$

where r is radial distance from the center of the sample and $B_{trapz}(r)$ is the axial direction ingredient of the trapped magnetic field.

The bulk superconductor disk with the radius of r_d, exposed to the external magnetic field and with the invasion depth of δ is assumed to be a coil of outer diameter $2r_d$, the inner diameter of $2(r_d-\delta)$, the height of h_d, and the self-inductance of $L(\delta)$. The total current I which flows in the bulk is shown as (2) using the shielding current distribution J_c, and is shown as (3) using the self-inductance $L(\delta)$. From (2) and (3), the formula (4) is drawn and the penetration depth is determined by solving this formula numerically (Komano, 2004).

$$I = J_c \delta h_d \tag{2}$$

$$I = \frac{\phi}{L(\delta)} \tag{3}$$

$$\delta L(\delta) = \frac{\phi}{h_0 J_c} \tag{4}$$

where φ is the total magnetic flux generated in the bulk and may be calculated from the well-known equation of $\varphi = \oint B.dS$, knowing the superconductor disk dimensions and the axial direction ingredient of the external magnetic field. The inductance $L(\delta)$, is calculated approximating the superconductor disk with a single-layer coil in cylindrical winding form, the details of which are presented by Grover (1946).

4. Levitation force

The levitation force may be calculated utilizing the Ampere's force density as (5) (Guo et al., 2007).

$$F_z = \iiint_{V_{SC}} (J_{SC} \times B).dV = \iiint_{V_{SC}} (J_{SC} \times B_{PM}).dV + \iiint_{V_{SC}} (J_{SC} \times B_{SC}).dV \tag{5}$$

where V_{sc}, J_{sc}, B_{PM} and B_{sc}, are the HTS volume, the super-current density, the magnetic flux density of PM, and the HTS flux density, respectively.

Since $\iiint_{V_{SC}} (J_{SC} \times B_{SC}).dV = 0$, (6) is obtained from (5) for the levitation force.

$$F_z = \iiint_{V_{SC}} (J_{SC} \times B_{PM}).dV \tag{6}$$

The levitation force should be equal to the disk weight modified to include the buoyancy of liquid nitrogen. Thus, (7) yields the required levitation force (Tsuda et al., 1998).

$$F_Z = (M_d - V_d \rho_{LN_2}) g \tag{7}$$

where M_d, V_d and ρ_{LN_2} are the mass of disk, the volume of disk and the density of liquid nitrogen, respectively.

5. Optimization process

The overall optimization process based on the simulated annealing heuristic method is shown in the flowchart of Fig. 3. In this process, the levitation force for a specific sample of PMG dimensions is calculated as discussed in part 4, based on the FEM simulation results of the PMG structures. The three PMG structures have been simulated as shown in Fig. 4, from which, the magnetic flux density distribution may be determined for any cross section along the PMG. The calculated levitation force is then compared to the required force for the levitation. The process is repeated and continues till an acceptable level of accuracy is obtained.

6. Results and discussion

The input data to the optimization process are the dimensions and characteristics of the superconductor disk and the levitation height while the outputs are the dimensions of the PMG structures. The optimization results are summarized in Tables 1, 2, 3, 4 for structure I, Tables 5, 6, 7, 8 for structure II, and Tables 9, 10, 11, 12 for structure III. The radius, height and the critical current density of the superconductor disk together with the levitation height have been determined as varying input parameters in these tables.

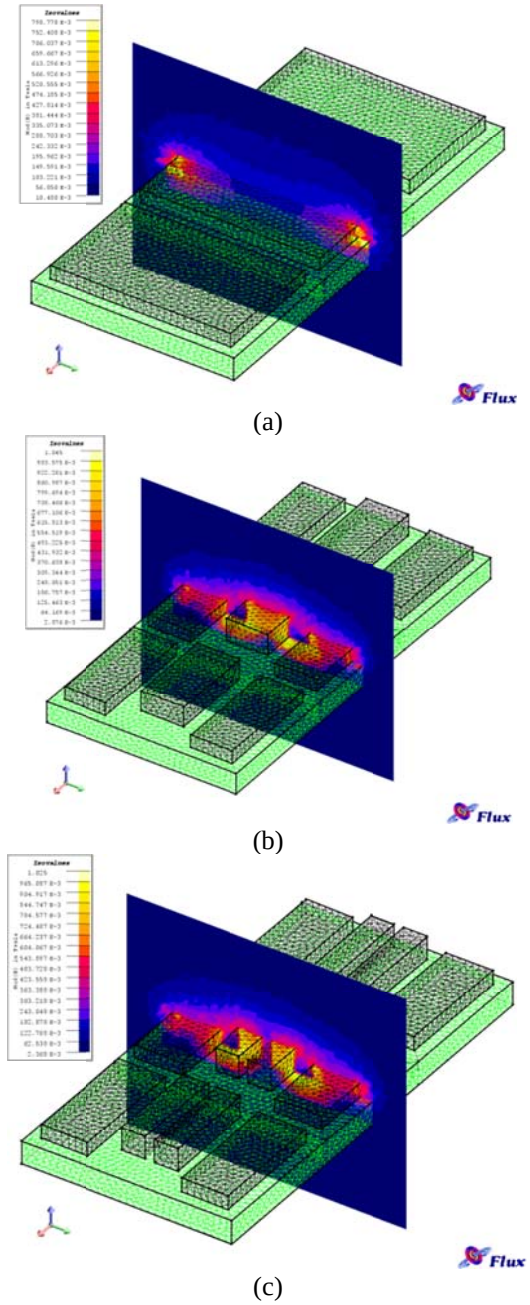

(a)

(b)

(c)

Fig. 4. Simulation of PMG structures in Flux 3D, a) Structure I, b) Structure II, c) Structure III

In each table three of the parameters have been assumed constant and only one parameter is varied. The optimum dimensions of the PMG calculated from the optimization process yield the minimum volume for the permanent magnets guaranteeing the satisfactory levitation performance of the PMG. According to the calculated PMG dimensions, two important characteristics for the PMG have been calculated and presented in the tables: volume of PMs per PMG length unit and the PMG width.

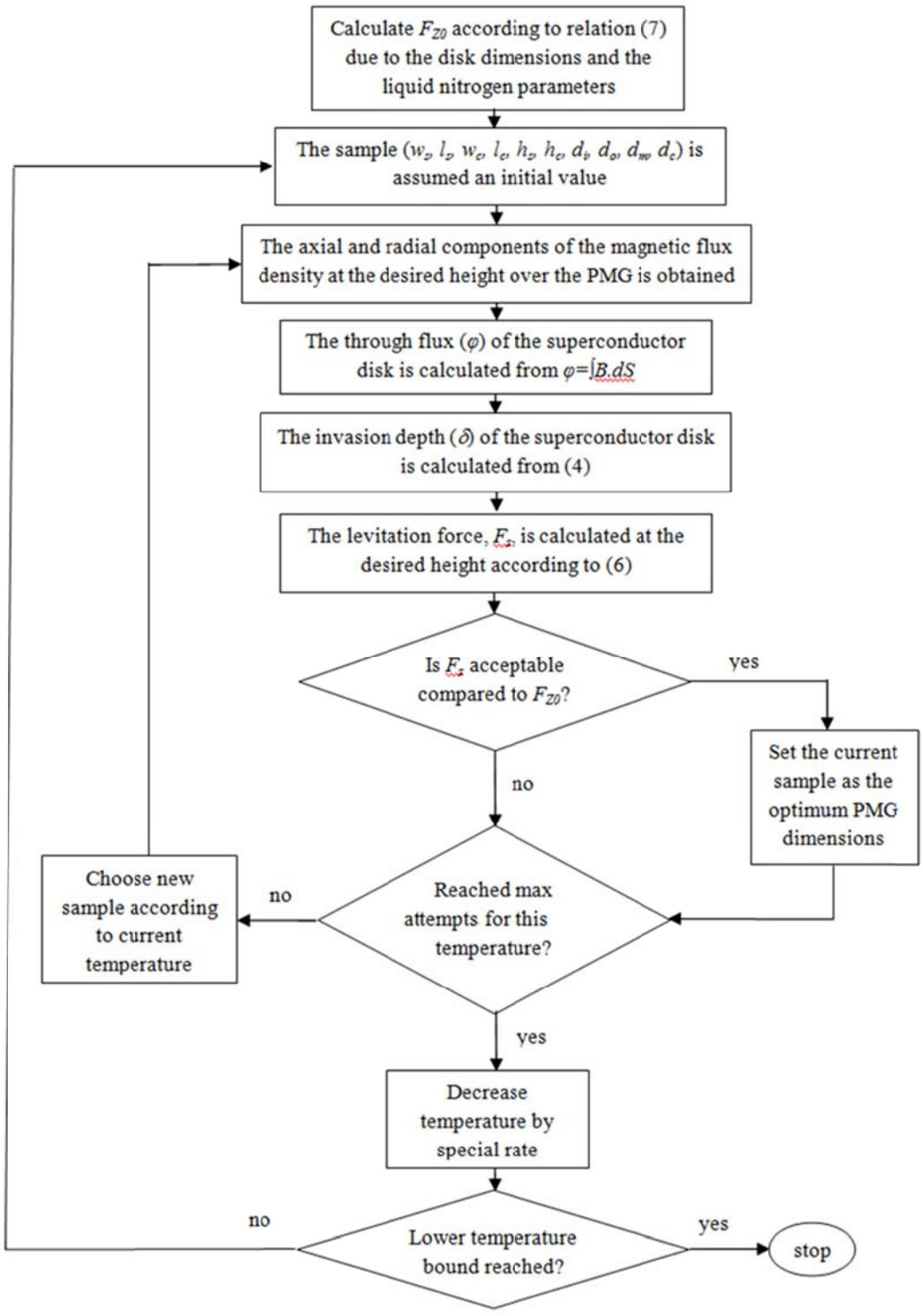

Fig. 3. The optimization flowchart

Table 1. The optimization result for the PMG dimensions in structure I, r_d is varied, J_c=10×10^6 A/m^2, h_0=10 mm, h_d=2 mm

r_d (mm)	4	6	8	10	12	14	16	18
w (mm)	27.8	35.0	46.8	62.5	81.0	106.6	126.5	148.0
l (mm)	20.2	25.5	29.3	34.1	39.0	44.2	49.0	53.1
h (mm)	3.8	4.6	5.3	6.2	7.2	8.0	8.7	9.3
d (mm)	4.2	4.7	5.3	5.9	6.4	7.0	7.5	8.1
magnets volume per PMG length (mm^3/m)	87455	135944	210046	330345	500987	736207	954460	1194229
PMG width (mm)	27.8	35.0	46.8	62.5	81.0	106.6	126.5	148.0

Table 2. The optimization result for the PMG dimensions in structure I, J_c is varied, r_d=8 mm, h_0=10 mm, h_d=2 mm

J_c×10^6 (A/m^2)	10	25	40	55	70	85	100	115
w (mm)	46.8	45.0	43.2	41.0	37.9	34.2	32.0	30.1
l (mm)	29.3	26.4	25.0	22.4	21.8	20.1	18.7	18.3
h (mm)	5.3	5.4	4.6	4.3	4.1	3.5	3.4	3.3
d (mm)	5.3	5.1	4.8	4.7	4.5	4.3	4.1	3.6
magnets volume per PMG length (mm^3/m)	210046	203657	166711	145723	128802	98607	89237	83000
PMG width (mm)	46.8	45.0	43.2	41.0	37.9	34.2	32.0	30.1

Table 3. The optimization result for the PMG dimensions in structure I, h_0 is varied, r_d=8 mm, J_c=10×10^6 A/m^2, h_d=2 mm

h_0 (mm)	4	6	8	10	12	14	16	18	20
w (mm)	39.2	42.5	45.6	46.8	55.0	61.5	70.0	76.3	92.1
l (mm)	26.2	27.2	28.0	29.3	30.1	31.9	34.6	39.4	44.7
h (mm)	4.3	4.5	5.1	5.3	5.9	6.4	6.9	7.5	8.3
d (mm)	4.4	4.7	5.0	5.3	5.6	6.2	6.5	6.9	7.4
magnets volume per PMG length (mm^3/m)	144324	163072	197324	210046	273599	329549	406613	486970	655854
PMG width (mm)	39.2	42.5	45.6	46.8	55.0	61.5	70.0	76.3	92.1

Table 4. The optimization result for the PMG dimensions in structure I, h_d is varied, r_d=8 mm, J_c=10×10^6 A/m^2, h_0=10 mm

h_d (mm)	1	2	3	4	5	6	7	8	9
w (mm)	44.5	46.8	52.1	54.6	58.4	62.9	68.7	75.2	80.6
l (mm)	26.8	29.3	32.1	35.2	39.9	42.2	47.1	50.4	54.6
h (mm)	4.2	5.3	6.5	7.9	9.3	10.5	11.9	14.2	15.5
d (mm)	4.9	5.3	5.5	5.8	6.0	6.3	6.7	7.0	7.3
magnets volume per PMG length (mm^3/m)	158010	210046	289114	370322	472124	574660	715719	937615	1101968
PMG width (mm)	44.5	46.8	52.1	54.6	58.4	62.9	68.7	75.2	80.6

Table 5. The optimization result for the PMG dimensions in structure II, r_d is varied, J_c=10×10^6 A/m^2, h_0=10 mm, h_d=2 mm

r_d (mm)	4	6	8	10	12	14	16	18
w_s (mm)	6.0	7.1	9.3	12.1	15.6	19.4	22.2	24
w_c (mm)	8.1	8.8	11.8	16.3	20.2	27	31.2	36
l_s (mm)	14.9	16.0	19.3	22.6	26.3	31.6	35.3	38.4
l_c (mm)	16.0	20.1	24.3	28.9	33.7	38.3	42.6	47.8
h_s (mm)	2.5	3	3.6	4.5	5	5.8	6.6	7.2
h_c (mm)	3.0	3.5	4.2	4.9	5.5	6.4	7.4	8.4
d_o (mm)	2.2	5.4	6.1	7.0	7.5	7.6	8.1	10.3
d_i (mm)	2.2	2.8	3.4	3.9	4.5	5.1	5.3	5.7
d_m (mm)	10.5	8.2	10.1	11.8	14.1	15.8	18.4	19.5
magnets volume per PMG length (mm^3/m)	48877	60780	98291	161128	235643	350242	464972	569318
PMG width (mm)	24.5	28.6	37.2	48.3	60.4	76.0	86.2	95.5

Table 6. The optimization result for the PMG dimensions in structure II, J_c is varied, r_d=8 mm, h_0=10 mm, h_d=2 mm

$J_c\times10^6$ (A/m^2)	10	25	40	55	70	85	100	115
w_s (mm)	9.3	9.1	8.8	8.5	8.1	7.5	6.8	6
w_c (mm)	11.8	11.5	11.0	10.4	9.8	9.0	8	7.1
l_s (mm)	19.3	18.6	17.8	16.8	15.8	14.6	13.5	12.2
l_c (mm)	24.3	22.0	20.2	18.6	16.9	15.6	14.1	13.5
h_s (mm)	3.6	3.3	2.8	2.3	1.8	1.7	1.5	1.3
h_c (mm)	4.2	3.5	2.9	2.3	1.7	1.8	1.9	1.7
d_o (mm)	6.1	4.2	4.0	4.1	3.6	3.3	3.0	2.9
d_i (mm)	3.4	3.5	3.2	3.0	2.9	2.7	2.5	2.4
d_m (mm)	10.1	10.3	9.4	8.6	8.0	7.5	6.9	6.5
magnets volume per PMG length (mm^3/m)	98291	87833	69798	52718	38263	34916	29679	23397
PMG width (mm)	37.2	36.7	35.0	33.4	31.8	29.4	26.6	23.9

Table 7. The optimization result for the PMG dimensions in structure II, h_0 is varied, r_d=8 mm, J_c=10×10^6 A/m^2, h_d= 2 mm

h_0 (mm)	4	6	8	10	12	14	16	18	20
w_s (mm)	8.4	8.7	8.9	9.3	9.8	10.5	11.5	13.0	14.8
w_c (mm)	10.5	10.8	11.3	11.8	12.5	13.4	14.7	16.7	19.4
l_s (mm)	18.3	18.5	18.8	19.3	20.4	21.7	23.3	25.9	29.5
l_c (mm)	21.7	22.3	23.2	24.3	25.8	27.7	30.1	32.9	36.3
h_s (mm)	3.1	3.2	3.4	3.6	3.8	4.1	4.5	4.9	5.4
h_c (mm)	3.0	3.3	3.8	4.2	4.7	5.1	5.7	6.2	6.9
d_o (mm)	3.5	4.0	5	6.1	5.7	6	7.4	7.1	6.8
d_i (mm)	2.7	2.9	3.1	3.4	3.7	3.9	4.2	4.6	4.8
d_m (mm)	8.7	9.2	9.5	10.1	10.3	10.8	12.2	13.6	15.2
magnets volume per PMG length (mm^3/m)	75073	81107	89664	98291	116287	135790	160703	203215	263758
PMG width (mm)	32.7	34.0	35.3	37.2	39.5	41.8	48.1	51.9	59.4

Table 8. The optimization result for the PMG dimensions in structure II, h_d is varied, r_d=8 mm, J_c=10×10^6 A/m^2, h_0=10 mm

h_d (mm)	1	2	3	4	5	6	7	8	9
w_s (mm)	8.7	9.3	9.9	10.4	11.1	11.9	12.9	14.1	15.2
w_c (mm)	11.2	11.8	12.2	12.7	13.2	13.9	14.9	16.0	17.3
l_s (mm)	18.1	19.3	20.0	21.1	22.3	23.5	24.8	26.2	27.5
l_c (mm)	23.0	24.3	25.3	25.5	26.7	27.9	29.5	30.3	31.1
h_s (mm)	2.5	3.6	4.5	5.7	6.7	7.6	8.9	10.5	12.4
h_c (mm)	2.9	4.2	5.3	6.5	7.8	9.0	10.6	12.3	13.8
d_o (mm)	5	6.1	5.5	4.6	4.9	5.1	5.3	5.6	5.8
d_i (mm)	3.7	3.4	3.2	3.1	2.8	2.6	2.5	2.3	2.1
d_m (mm)	9.7	10.1	10.5	11.3	12.0	12.3	13.1	13.5	14.6
magnets volume per PMG length (mm^3/m)	66424	98291	134035	179245	223011	270664	343980	431475	534270
PMG width (mm)	36	37.2	38.4	39.7	41.0	42.9	45.7	48.8	51.9

Table 9. The optimization result for the PMG dimensions in structure III, r_d is varied, J_c=10×10^6 A/m^2, h_0=10 mm, h_d=2 mm

r_d (mm)	4	6	8	10	12	14	16	18
w_s (mm)	6.1	8.4	10.6	13.3	17.1	21.1	24.2	26.4
w_c (mm)	5.1	5.2	7.6	9.8	12.0	16.1	21.0	21.5
l_s (mm)	14.2	14.8	21.4	24.0	28.8	35.0	45.3	48.7
l_c (mm)	19.0	20.0	23.8	26.0	34.1	40.8	52.1	54.8
h_s (mm)	2.8	3.4	4.0	5.2	5.6	6.5	7.1	8.0
h_c (mm)	3.8	4.3	5.2	6.0	6.7	7.8	9.1	10.3
d_o (mm)	5.0	5.2	4.5	4.9	5.5	6.3	7	6.3
d_i (mm)	1.4	2.3	1.7	3.9	3.2	6	3.4	9.9
d_m (mm)	7.5	8.5	11.2	13.4	14.9	14.8	17.8	21.8
d_c (mm)	1.5	2.9	4.1	5.2	6.4	7.7	9.1	10.4
magnets volume per PMG length (mm^3/m)	63620	86990	142699	220668	320674	480576	678385	815306
PMG width (mm)	26.7	34.7	43.9	59.2	71.0	94.1	106.3	126.0

Table 10. The optimization result for the PMG dimensions in structure III J_c is varied, r_d=8 mm, h_0=10 mm, h_d=2 mm

J_c×10^6 (A/m^2)	10	25	40	55	70	85	100	115
w_s (mm)	10.6	10.3	9.5	9.2	8.1	7.5	6.8	7.6
w_c (mm)	7.6	7.3	7.3	6.7	6.5	6.0	5.8	3.8
l_s (mm)	21.4	20.7	19.4	18.5	17.0	15.8	15.2	14.0
l_c (mm)	23.8	22.0	20.2	19.6	17.5	16.5	16.0	15.2
h_s (mm)	4.0	3.9	3.9	3.6	2.8	3.0	2.7	2.5
h_c (mm)	5.2	4.5	4.1	3.8	3.5	3.6	3.1	3.3
d_o (mm)	4.5	4.2	4.1	3.7	3.4	3.0	3.2	3.1
d_i (mm)	1.7	1.5	1.4	1.5	1.2	1.1	1.1	1.0
d_m (mm)	11.2	11.0	10.5	9.6	9.2	8.7	8.3	8.0
d_c (mm)	4.1	3.8	3.5	3.6	3.3	3.0	2.7	2.5
magnets volume per PMG length (mm^3/m)	142699	124835	112626	100158	76833	75734	61603	53404
PMG width (mm)	43.9	41.9	39.9	38.4	34.8	32.1	30.0	27.3

Table 11. The optimization result for the PMG dimensions in structure III h_0 is varied, r_d=8 mm, J_c=10×10^6 A/m^2, h_d= 2 mm

h_0 (mm)	4	6	8	10	12	14	16	18	20
w_s (mm)	9.2	9.7	10.0	10.6	11.4	12.5	13.7	14.9	16.0
w_c (mm)	6.7	7.5	7.9	7.6	8.8	9.1	10.2	12.8	13.6
l_s (mm)	17.6	18.4	19.5	21.4	22.4	23.8	25.6	28.5	32.8
l_c (mm)	20.1	21.0	22.5	23.8	25.2	27.9	31.5	34.9	38.3
h_s (mm)	3.6	3.8	3.6	4.0	4.5	5.1	5.5	6.2	7.1
h_c (mm)	4.0	4.3	4.8	5.2	5.7	6.5	7.0	7.6	8.0
d_o (mm)	3.6	4.0	4.2	4.5	4.7	5.1	5.9	6.5	5.7
d_i (mm)	1.2	1.4	1.6	1.7	1.9	2.0	2.4	2.8	2.5
d_m (mm)	9.5	10.2	10.8	11.2	11.5	11.8	12.8	14.3	16.4
d_c (mm)	2.8	3.6	3.3	4.1	3.9	4.2	4.4	4.8	5.1
magnets volume per PMG length (mm^3/m)	105811	121022	131241	142699	178092	219208	265270	344451	410031
PMG width (mm)	37.0	40.8	42.3	43.9	44.2	51.4	56.9	65.8	68.1

Table 12. The optimization result for the PMG dimensions in structure III h_d is varied, r_d=8 mm, J_c=10×10^6 A/m^2, h_0=10 mm

h_d (mm)	1	2	3	4	5	6	7	8	9
w_s (mm)	9.6	10.6	11.2	11.4	12.5	13.3	14.2	15.4	16.8
w_c (mm)	7.0	7.6	8.0	8.5	9.1	9.3	9.5	10.0	10.2
l_s (mm)	20.0	21.4	22.0	22.9	24.0	26.7	26.9	28.5	30.0
l_c (mm)	23.1	23.8	26.3	26.5	26.8	28.9	29.5	30.6	33.7
h_s (mm)	3.0	4.0	5.5	6.6	7.1	8.2	9.3	11.2	13.4
h_c (mm)	4.1	5.2	6.4	7.4	8.3	9.6	10.9	12.6	15.0
d_o (mm)	4.3	4.5	4.7	4.9	5.0	5.3	5.7	6.1	6.4
d_i (mm)	1.3	1.7	2.2	2.8	3.3	3.8	4.5	4.6	5.4
d_m (mm)	10.7	11.2	11.5	12.5	13.1	13.5	14.3	15.0	15.6
d_c (mm)	4.0	4.1	3.9	3.5	3.8	3.4	3.1	2.8	2.7
magnets volume per PMG length (mm^3/m)	101971	142699	202378	243874	286497	343256	405347	507012	654379
PMG width (mm)	39.8	43.9	46.7	48.9	53.6	56.2	59.5	62.8	67.5

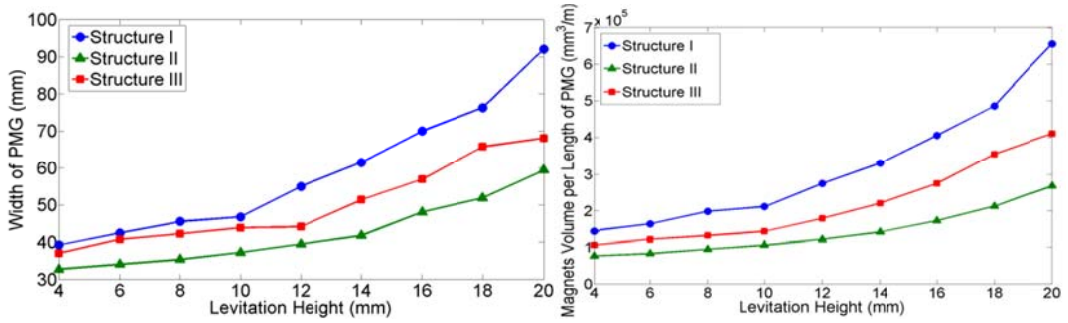

(a)

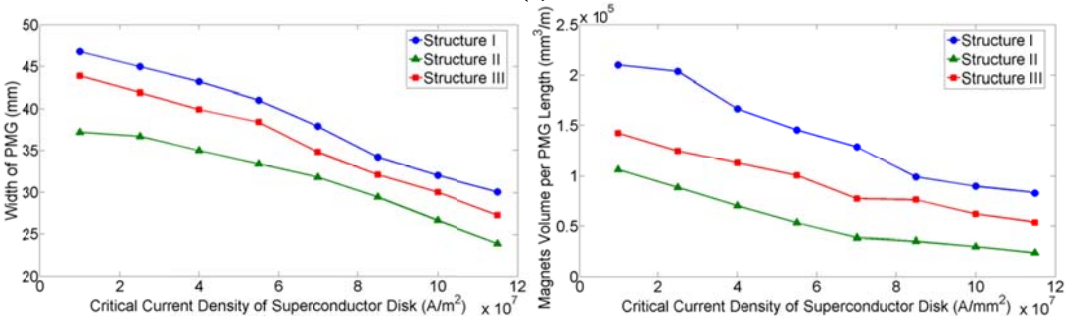

(b)

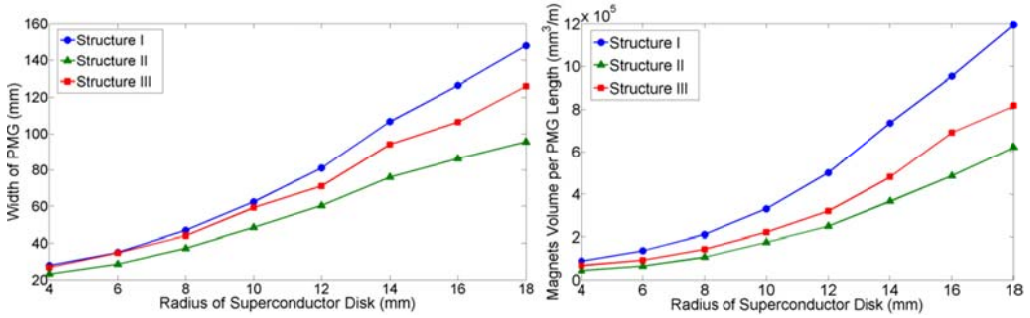

(c)

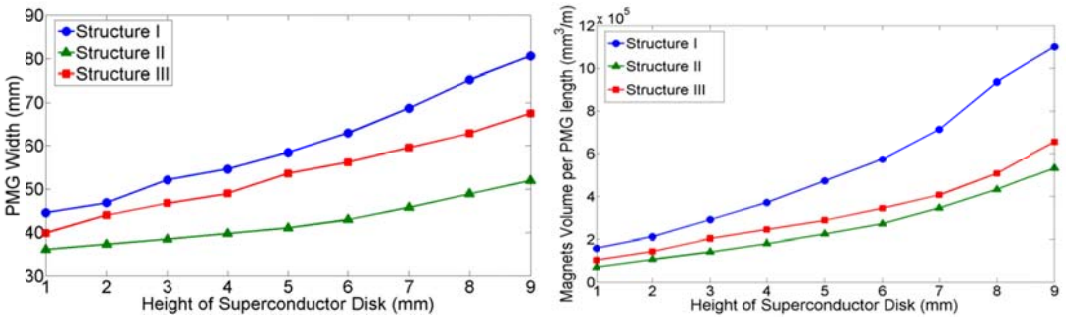

(d)

Fig. 5. The variation of the PMG width and the PMs volume with: a) levitation height, h_0, b) critical current density, J_c, c) radius, r_d, and d) height ,h_d, of the superconductor disk

6.1. Permanent magnets volume per PMG length

Permanent magnets volume per PMG length unit is calculated as the volume of the PMs in the longitudinal sample of PMG divided by the length of the sample. In other words, it is a measure for the volume of the permanent magnets per unit length of the PMG, and as a result, a measure of the PMG cost. It may be calculated as (8), (9) and (10) for the three structures I, II and III, respectively.

$$\textit{PMs volume per PMG length unit of structure I} = \frac{w \times l \times h}{l + d} \tag{8}$$

$$\textit{PMs volume per PMG length unit of structure II} = \frac{2 \times w_s \times l_s \times h_s + w_c \times l_c \times h_c}{l_s + d_o} \tag{9}$$

$$\textit{PMs volume per PMG length unit of structure III} = \frac{2 \times w_s \times l_s \times h_s + 2 \times w_c \times l_c \times h_c}{l_s + d_o} \tag{10}$$

6.2. PMG width

PMG width is obtained from the calculated optimum PMG dimensions and is important due to creation of the moving band for the superconductor disk. It is calculated as (w) for PMG structure I, as ($2w_s+2d_i+w_c$) for the structure II and as ($2w_s+2d_i+2w_c+dc$) for the structure III.

The variation of the width and the volume of the permanent magnets in three structures of PMG versus the parameters of the superconductor disk such as its radius r_d, critical current density J_c, height h_d, and the levitation height h_0, are shown in Fig. 5. It may be deduced that increasing the levitation height and the radius and the height of the superconductor disk, considerably increase the width of the PMG and the volume of the permanent magnets used per length unit of the PMG. Increasing the critical current density of the superconductor disk decreases the volume of the permanent magnets used per length unit of the PMG because increasing the critical current density, the shielding super-currents increase in the superconductor disk and as a result, lesser PMG width and PM volume are required for a specific levitation force.

The structure II seems to be the most desirable structure from an economical point of view as it results in the least volume of the permanent magnets and also with the least width of PMG. The structure III is next and the structure I is the most expensive structure.

6.3. Fabricated PMG Prototypes

Prototype guideways with the resulted dimensions have been fabricated for the superconductor disk with the dimensions and characteristics as mentioned in part 2. Practical tests are performed with the levitation height of 1 cm and show satisfying results. A typical constructed PMG is shown in Fig. 6.

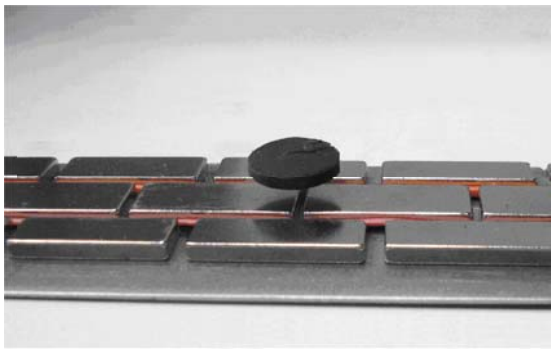

Fig. 6. The typical constructed PMG

The balance of the disk in motion and the maximum allowable speed (especially in twisted guideways) may be compared for the three structures. Experiments show that the structure III provides the most stable motion for the

superconductor disk. This may be due to the magnetic field dip at the middle of the PMG. This magnetic flux density dip creates a trap for the superconductor disk and causes the superconductor disk not to slide aside. The structure I shows the weakest stability behavior of the disk and the superconductor disk simply slides outside the guideway at higher speeds.

7. Summary and conclusion

In this paper, a process is proposed to yield the optimum design of the permanent magnet guideways for different levitation heights and the superconductor disk characteristics and dimensions. The influence of varying these parameters on the PMG design and characteristics has also been presented. The levitation force between HTS and PM is analyzed by using axisymmetric 3D FEM. These results may provide basic analysis for the optimized HTS-PMG levitation systems. prototype guideways have also been fabricated and tested successfully. PMG structures other than those studied in this paper are possible and may be considered, especially from the viewpoint of superconductor disk stability on the permanent magnet guideway.

References

Alvaro, S., & Carles, N. (2001). Levitation force between a superconductor and a permanent magnet with cylindrical symmetry. *Physica C: Superconductivity and its Applications*, 364–365, 360–362.

Andrade, R., & et al. (2003). Performance of Nd-Fe-B and ferrite magnets in superconducting linear bearings with bulk YBCO. *IEEE Transactions on Applied Superconductivity*, 13, 2271–2274.

Brandt, E. H. (1988). Friction in levitated superconductors. *Applied Physics Letters*, 53, 1154–1556.

Cha, Y. S., Hull, J. R., Mulcahy, T. M., & Rossing, T. D. (1991). Effect of size and geometry on levitation force measurements between permanent magnets and high temperature superconductors. *Journal of Applied Physics*, 70, 6504–6506.

Del-Valle, N., Sanchez, A., Pardo, Chen, E., & Navau, D. X., (2007). Enhanced stability by field cooling in superconducting levitation with translational symmetry. *Applied Physics Letters*, 91, 112507.

Del-Valle, N., Sanchez, A., Pardo, E., Chen, D. X., & Navau, C. (2007). Optimizing levitation force and stability in superconducting levitation with translational symmetry. *Applied Physics Letters*, 90, 042503.

Del-Valle, N., Sanchez, A., Navau, C., & Chen, D. X. (2008). Lateral-displacement influence on the levitation force in a superconducting system with translational symmetry. *Applied Physics Letters*, 92, 042505.

Deng, Z., Lin, Q., Ma, G., Zheng, J., Zhang, Y., Wang, S., & Wang, J. (2008). A Double-Superconducting Axial Bearing System for an Energy Storage Flywheel Model. Journal of Physics: *Conference Series*, 97, 012283.

Fukai, H., Tomita, M., Murakami, M., & Nagatomo, T. (2000). Jc-B properties of large RE-Ba-Cu-O disks. *Superconductor Science and Technology*, 13, 798-801.

Fukai, H., Tomita, M., Murakami, M., & Nagatomo, T. (2001). Numerical simulation of trapped magnetic field for bulk superconductor. *Physica C: Superconductivity and its Applications*, 357–360, 774–776.

Grilli, F., Stavrev, S., Le Floch, Y., Costa-Bouzo, M., Vinot, E., Klutsch, L., Meunier, G., Tixador, P., & Dutoit, B. (2005). Finite Element Method Modelling of Superconductors: from 2D to 3D. *IEEE Transactions on Applied Superconductivity*, 15, 17–25.

Grover., F. W. (1946). *Inductance Calculations: Working Formulas and Tables*. New York: Dover Publications Incorporation.

Guo, Y., Jin, J. X., Zhu, J. G., & Lu, H. Y. (2007). Design and Analysis of a Prototype Linear Motor Driving System for HTS Maglev Transportation. *IEEE Transactions on Applied Superconductivity*, 17(2), 2087–2090.

Hashizume, H., Toda, S., & Maeda, K. (1996). Numerical evaluation of electromagnetic force induced in high T_c superconductor with grain boundary. *IEEE Transactions on Magnetics*, 32(3), 1148–1151.

Hekmati, A., & et al. (2012). A novel method of flat YBCO rings development for shield-type superconducting fault current limiters fabrication. *Physica C: Superconductivity and its Applications*, 472, 39–43.

Hull, J. R. (2000). Superconducting bearings. *Superconductor Science and Technology*, 13, R1-R15.

Brandt, E. H. (1989). Levitation in physics, Science, 243, 349–355.

Iwasa, Y., Lee, H., Sawa, K., & Murakami, M. (1997). Active magnetic levitation with YBCO samples. Advances in Superconductivity IX: *Proceedings of the ninth International Symposium on Superconductivity*, 2, 1379.

Komano, Y., & et al. (2004). Numerical simulation of levitation force and magnetic field in levitated bulk superconductor. *Physica C: Superconductivity and its Applications*, 412–414, 729–733.

Kovalev, L. K., & et al. (2002). high output power reluctance electric motors with bulk high-temperature superconductor elements. *Superconductor Science and Technology*, 15, 817–822.

Kuehn, L., Mueller, M., Schubert, R., Beyer, C., de Haas, O., & Schultz, L. (2007). Static and dynamic behavior of a superconducting magnetic bearing using YBCO bulk material. *IEEE Transactions on Applied Superconductivity*, 17, 2079–2082.

Ma, G. T., Lin, Q. X., Wang, J. S., Wang, S. Y., Deng, Z. G., Lu, Y. Y., Liu, M. X., & Zheng, J. (2008). Method to reduce levitation force decay of the bulk HTSC above the NdFeB guideway due to lateral movement. *Superconductor Science and Technology*, 21, 065020.

Ma, K. B., Postrekhin, Y. V., & Chu, W. K. (2003). Superconductor and magnet levitation devices. *Review of Scientific Instruments*, 74, 4989–5017.

Matsunaga, M., & et al. (2002). YBCO bulk for the superconducting bearing for a 10kWh flywheel. *Superconductor Science and Technology*, 15, 842–845.

Minami, H., & Yuyama, J. (1995). Construction and Performance Test of a Magnetically Levitated Transport System in Vacuum Using High-T_c Superconductors. *Japanese Journal of Applied Physics*, 34, 346–349.

Moon, F. C. (1994). *Superconducting Levitation*. New York: Wiley.

Nagashima, K., Higuchi, T., Sok, J., Yoo, S. I., Fujimoto, H., & Murakami, M. (1997). The trapped field of YBCO bulk superconducting magnets. *Cryogenics*, 37, 577–581.

Nagaya, S., Kashima, N., Minami, M., Kawashima, H., Unisuga, S., Kakiuchi, Y., & Ishigaki, H. (2001). Study on characteristics of high temperature superconducting magnetic thrust bearing for 25 kWh flywheel. *Physica C: Superconductivity and its Applications*, 357–360, 866-869.

Oka, T., & et al. (2000). Construction of a 2–5 T class superconducting magnetic field generator with use of an Sm123 bulk superconductor and its application to high-magnetic field demanding devices. *Physica C: Superconductivity and its Applications*, 335, 101–106.

Oswald, B., Krone, M., Straßer, T., Best, K. -J., Söll, M., Gawalek, W., Gutt, H. J., Kovalev, L., Fisher, L., Fuchs, G., Krabbes, G., & Freyhardt, H. C. (2002). Design of HTS reluctance motors up to several hundred kW. *Physica C: Superconductivity and its Applications*, 372-376, 1513–1516.

Putman, P. T., Zhou, Y. X., Fang, H., Klawitter, A., Salama, K. (2005). Application of melt-textured YBCO to electromagnetic launchers. *Superconductor Science and Technology*, 18, S6–S9.

Ren, Z., Wang, J., Wang, S., Jiang, H., Zhu, M., Wang, X., & Song, H. (2003). Influence of shape and thickness on the levitation force of YBaCuO bulk HTS over a NdFeB guideway. *Physica C: Superconductivity and its Applications*, 384, 159–162.

Rubinacci, G., Villone, F., & Zamboni, W. (2004). Power-law characteristic for 3D macroscopic modeling of superconductors via an integral formulation. *IEEE Transactions on Magnetics*, 40(2), 900–903.

Schultz, L., de Haas, O., Verges, P., Beyer, C., Rohlig, S., Olisen, H., Kuhn, L., Berger, D., Noteboom, U., & Funk, U. (2005). Superconductively levitated transport system–The SupraTrans project. *IEEE Transactions on Applied Superconductivity*, 15, 2031–2035.

Song, H., Zheng, J., Liu, M., Zhang, L., Lu, Y., & et al. (2006). Optimization and design of the permanent magnet guideway with the high temperature superconductor. *IEEE Transactions on Applied Superconductivity*, 16, 1023–1026.

Stumberger, G., Aydemir, M. T., Zarko, D., & Lipo, T. A. (2004). Design of a linear bulk superconductor magnet synchronous motor for electromagnetic aircraft launch systems. *IEEE Transactions on Applied Superconductivity*, 14, 54–62.

Tamegai, T., Iye, Y., Oguro, I., & Kishio, K. (1993). Anomalous peak effect in single crystal $Bi_2Sr_2CaCu_2O_{8+y}$ studied by Hall probe magnetometry. *Physica C: Superconductivity and its Applications*, 213, 33–42.

Tsuchimoto, M., Kojima, T., & Honma, T. (1994). Numerical analysis of frozen field model for levitation force of HTSC. *Cryogenics*, 34(10), 821–824.

Tsuda, M., Lee H., & Iwasa, Y. (1998). Electromaglev (active-maglev)–magnetic levitation of a superconducting disk with a DC field generated by electromagnets: Part 3. Theoretical results on levitation height and stability. *Cryogenics*, 38, 743–756.

Wang, J., Wang, S., Zeng, Y., Huang, H., Luo, F., & et al. (2002). The first man-loading high temperature superconducting Maglev test vehicle in the world. *Physica C: Superconductivity and its Applications*, 378–381, 809–814.

Wang, J., Wang, S., Deng, C., Zheng, J., Song, H., He, Q., & et al. (2007). Laboratory scale high temperature superconducting Maglev launch system. *IEEE Transactions on Applied Superconductivity*, 17, 2091–2094.

Wang, J., & et al. (1999). A scheme of maglev vehicle using high Tc bulk superconductors. *IEEE Transactions on Applied Superconductivity*, 9, 904–907.

Wang, J., Wang, S., & Zheng, J. (2009). Recent Development of High Temperature Superconducting Maglev System in China. *IEEE Transactions on Applied Superconductivity*, 19, 2142–2147.

Weinberger, B. R., Lynds, L., Hull, J. R., & Balachandran, U. (1991). Low friction in high temperature superconductor bearings. *Applied Physics Letters*, 59, 1132-1134.

Yang, W., Qiu, M., Liu, Y., Wen, Z., Duan, Y., & Chen, X. (2007). Levitation characteristics in an HTS Maglev launch assist test vehicle. *Superconductor Science and Technology*, 20, 281–286.

Yang, W. J., Wen, Z., Duan, Y., Chen, X. D., Qiu, M., Liu, Y., & Lin, L. Z. (2006). Construction and performance of HTS Maglev launch assist test vehicle. *IEEE Transactions on Applied Superconductivity*, 16, 1108–1111.

Yoo, S. I., Higuchi, T., Sakai, N., Fujimoto H., & Murakami, M. (1998). RE-Ba-Cu-O for high functional superconducting permanent magnet. *Materials Science and Engineering: B*, 52, 203–210.

Zhang, Y., Xu, S., & Jin, N. (1998). Experiment analysis of a HTSC Maglev vehicle model. *Advanced Technology of Electrical Engineering and Energy*, 17, 51–54.